Hindawi
Advances in Materials Science and Engineering
Volume 2019, Article ID 8643608, 15 pages
https://doi.org/10.1155/2019/8643608

Research Article

Aesthetic and Mechanical Suitability of a Clear Synthetic Resin as a Unconventional Binder for Road Pavements

Marco Pasetto, Andrea Baliello, Giovanni Giacomello, and Emiliano Pasquini

Department of Civil, Environmental and Architectural Engineering, University of Padova, Padova 35131, Italy

Correspondence should be addressed to Marco Pasetto; marco.pasetto@unipd.it

Received 29 March 2019; Revised 13 May 2019; Accepted 18 May 2019; Published 23 June 2019

Guest Editor: Jose Norambuena-Contreras

Current environmental awareness interests several aspects of civil engineering, including road construction. Indeed, new challenges related to environmental pollution and landscape preservation must be faced. In this sense, clear road pavement surfaces represent an effective technology aimed at guaranteeing environmental-friendly aesthetic pavements. The use of clear synthetic resin as a binder involves several benefits for the mitigation of in-service reached temperatures and the heat distribution within pavements (with appreciable effects on pavement mechanical performance too). The present paper illustrates an experimental study aimed at analysing the chromatic and mechanical properties of a clear synthetic resin and thus its suitability as a binder for road pavement mixes. Chromatic characteristics were assessed through digital image analysis at different aging conditions. A dynamic shear rheometer was used to evaluate the linear viscoelastic properties as well as fatigue and rutting potential of the binder in a wide range of temperatures and frequencies. A conventional 35/50 penetration grade bitumen was also investigated for comparison purposes. The clear resin exhibited limited changes in colour (darkening effects), mainly in the case of short-term aging. On the other hand, a low temperature-dependency of such a binder was observed up to 58°C. Slightly increased aptitude to rutting at the higher temperatures was detected, even if it is worth noting that clear in-service mixtures would achieve lower temperatures than traditional "black" materials at a given environmental condition (air temperature, solar radiation, etc.). The resin also exhibited a softer behaviour, along with an enhanced fatigue resistance. Overall, the studied innovative binder showed promising results in view of its effective use in road paving.

1. Introduction

Actually, environmental awareness interests the most part of our society, and it especially concerns the civil construction field. Road construction is a core sector, since road pavements are widely diffused involving huge amounts of materials. In particular, they cover considerable surfaces in urban areas, where their dark colour negatively contributes to the quality of the environment [1]. Therefore, a growing attention is paid to the implementation of new materials for road surfaces (i.e., coloured-aesthetic pavements) able to promote the landscape preservation [2, 3]. Initially, these solutions were principally aimed at fulfilling specific safety requirements complying with the needs of eco-friendly design and realization of pavements. Recently, applications of clear or coloured pavements were proposed also as a way to mitigate the heat concentration within anthropized environments which causes the so-called Urban Heat Island (UHI) phenomenon.

UHI effect is related to the different air temperatures observed between cities and rural regions; they highlight the seasonal and daily dynamics of local heating and global warming (average temperature of earth and atmosphere/climatic changes). UHI is a complex phenomenon affected by many variables, for example, related to urban space morphology composing the texture of the town (dimensional ratios of items, sky view factor, orientation of urban texture, presence of urban canyon, etc.). Furthermore, urban microclimate is characterized by considerable time and space variations of environment conditions; this is due to different material types and depends on several factors such as air temperature, relative humidity, wind (speed and type), solar radiation (direct sunlight and diffuse light), and infrared surface radiation (heat released). Thus, research

studies concerning urban heat islands mitigation strategies are of fundamental importance and involve multidisciplinary expertise.

In regard to this issue, since the detrimental increase in temperature is mainly related to the large presence of nonreflective and high-absorbing surfaces, optimized solutions for road construction (clear or coloured pavements) could effectively contribute to the reduction of heat concentration and diffusion (i.e., mitigation of the UHI effects), thus improving the human health and the life quality [4–6]. In fact, it is well known that the thermal properties of the materials such as the albedo (reflected energy of solar shortwave radiation), the emissivity (ratio of the radiant energy emitted by the surface to that emitted by a black element), and the Solar Reflex Index (SRI, ability to maintain a cool temperature) are related to the colour and the texture of the surfaces [5–8]. Thus, the importance of road surfaces in the UHI phenomenon is crucial since, as anticipated, roads cover a significant part of urban areas and are traditionally manufactured with black/dark high-emissivity materials which strongly enhance heat absorption and diffusion [9, 10]. Moreover, several studies also reported that clear/coloured pavements are able to guarantee benefits in road illumination, night visibility, driving safety, and, for given light conditions, cost savings (especially in road tunnels); moreover, the use of synthetic binders can also reduce the increasing consumption of the petroleum reserves [2], thus enhancing the related environmental benefits.

According to the literature [11–15], clear binders are generally constituted by adhesive materials (having similar mechanical properties with respect to the bitumen) characterized by a yellowish/transparent colour. Regardless of different formulations and peculiarities, such synthetic products cover a significant part of the clear binder market. It is worth specifying that they totally differ from clear modified bitumens, which are obtained by the extraction of the asphaltenes (responsible of the dark colour).

Given this introduction, the aim of the present research is addressed to the analysis of the suitability of a clear synthetic resin to be used as a binder for road pavement mixes instead of traditional bitumen. Given the fact that little research exists on clear, coloured, or solar-reflective road materials for UHI mitigation [16–18], this paper would like to enlarge the existing literature, representing the preliminary phase of a comprehensive research program aimed at developing high-reflective pavements for UHI mitigation with the final goal of a proper quantification of cooling benefits due to pavement chromatic characteristics. Even if the clear colour of the studied material can strongly affect in-service temperatures, heat distribution within the pavement, and its diffusion into the environment, the mixes prepared with such a binder can be used only if they are also able to guarantee adequate mechanical properties and durability as well as to preserve chromatic characteristics over time. Thus, the present paper shows the results of an experimental characterization of clear synthetic resin in comparison of a traditional bitumen: the first phase of the study concerned the evaluation of chromatic characteristics of the resin and the effect of aging processes on these characteristics, whereas the second phase dealt with a comparative rheological characterization of resin and bitumen evaluating the linear viscoelastic properties as well as the fatigue and rutting potentials.

2. Materials and Methods

2.1. Materials. The studied clear synthetic resin (hereafter coded CSR) was a proprietary product composed by a thermoplastic bicomponent resin (solid granular elements and liquid catalyst) with bonding properties similar to those of a traditional bitumen. The colour of the material varies from amber-orange to straw-yellow. Such a binder can allow the preparation of clear or coloured pavement surfaces since it can be used instead of the traditional black bitumen (dosed with similar volumetric contents) and by utilizing the same conventional preparation and construction paving procedures (plants, equipment, etc.). A reference unmodified bitumen with a 35/50 penetration grade (hereafter coded 35/50 pen) was also studied for comparison purposes.

Table 1 summarizes the main basic properties of CSR and 35/50 pen. Based on these basic characteristics, CSR demonstrated a noticeably lower consistency at midservice temperature, whereas it seemed to be less temperature-dependent with higher short-term aging resistance. Moreover, a noticeably higher elastic response was observed in the case of the synthetic binder. A reduced ductility is also reported, and a higher thermal cracking potential can be also hypothesized due to the higher Fraass breaking point. A specific rheological study would be recommended in this regard.

2.2. Chromatic Analysis. The first phase of the research was aimed at assessing the chromatic characteristics of the studied binders, with particular emphasis on the aging effects on the clear binder colour. Thus, CSR samples were replicated as unaged resin, RTFO resin (short-term aging simulation—EN 12607-1), and PAV resin (long-term aging simulation—EN 14769). The 35/50 pen sample was also studied for comparison purposes. To prepare the test samples, materials were first oven-heated at 160°C and poured into circular glass containers in order to obtain specimens with a layer thickness able to prevent the transparency (i.e., 1.0 mm). The specimens were then placed in a confined chamber, opportunely set up to achieve high-quality images. The setup was composed by a rectangular box ($1000 \times 800 \times 700$ mm) with white paper walls useful to permit the light transition. Four light sources were placed on the sides of the box in order to prevent shades or reflections. A centred circular hole ($\Phi = 300$ mm) on the upper side of the box allowed the image acquisition using a digital high-resolution camera. Additional details concerning chamber setup are reported in Figure 1. In order to acquire images not affected by different exposures or light noises, all samples (35/50 pen, unaged CSR, RTFO-aged CSR, and PAV-aged CSR) were contemporarily photographed in the same picture.

Table 1: Basic properties of tested binders.

Property	Standard	35/50 pen	CSR
Penetration at 25°C (0.1 mm)	EN1426	38	69
Penetration at 25°C after RTFO (0.1 mm)	EN1426	23	54
Softening point (°C)	EN1427	65	61
Softening point after RTFO (°C)	EN1427	72	64
Penetration index	EN12591	1.3	2.1
Ductility at 25°C (mm)	ASTM D-113	>1000	210
Elastic recovery (%)	EN13398	9	91
Fraass breaking point (°C)	EN12593	−5.8	−7.5

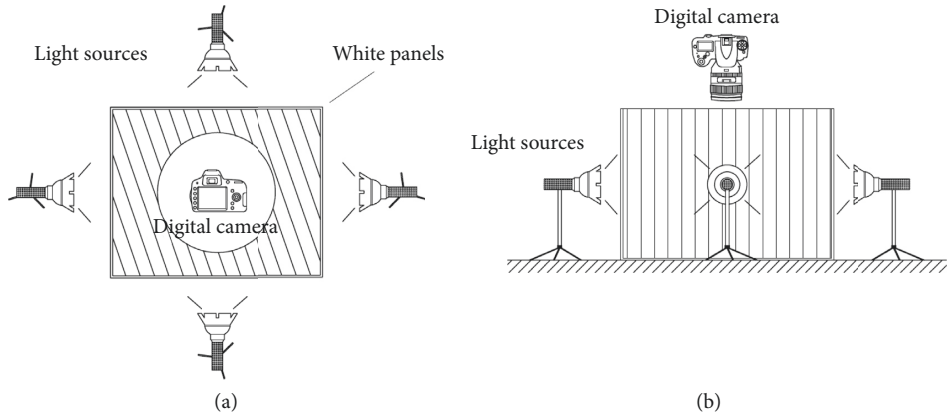

Figure 1: Confined chamber for image acquisition: top (a) and side (b) views.

A back analysis was performed with specific graphic software to determine material RGB (Red-Green-Blue) properties. RGB colour model (described by Commission Internationale de l'Éclairage since the 1931) is a common representation to display images in electronic/photographic systems that reproduce an array of colours from the three primary colours (red, green, and blue). In this way, the single colour could be represented by the numerical triad R-G-B (with digits ranging between 0 and 255 intervals), where each number indicates the mean value of the Gauss distribution for each colour. As a consequence, an image with limited chromatic variations could define localized curve distributions, improving the dominant RGB code accuracy (small standard deviations in Gauss curves). For this reason, the target of the picture acquisition was a high-resolution clean image, not influenced by reflections, shades, or flaws. However, an alternative analysis that considered an objective physical representation (based on human perception) was also proposed, since RGB actually defines a device-dependent colour model, not strictly related to an engineering property.

Colour perception is linked to the perceptive feedback of the optical system in relationship with electromagnetic light stimuli. Considering the eye composition with three retinal photoreceptor cones, three numerical functions are enough to model the colours. In this regard, the Hue-Saturation-Lightness (HSL) model was used, since it represents one of the most utilized models based on human perception of colours [19, 20]. According to this model, the parameter hue (H) reproduces the colour tonality (in the range of 0°–360°), the saturation (S) indicates the power of light emission (as percentage), and the lightness (L) represents the colour brightness (as percentage). Thus, the conversion from RGB to HSL values was developed through the following steps according to [21]: (i) expressing red, green, and light values in the range between 0 and 1 (dividing RGB digits by 255); (ii) identifying the minimum (min) and maximum (max) normalized RGB values; (iii) following the mathematical procedure hereafter reported (equations (1)–(3d)).

Figure 2 illustrates the RGB and HSL model's interpretation in a 3D space. Once the HSL codifications for unaged, RTFO-aged, and PAV-aged resin samples are defined, comparisons to understand the aging effects on their chromatic characteristics were carried out.

$$L = 100 \cdot \frac{(\max + \min)}{2}, \tag{1}$$

$$S = 100 \cdot \frac{(\max - \min)}{\max + \min}, \quad \text{if } L \leq 0.5, \tag{2a}$$

$$S = 100 \cdot \frac{(\max - \min)}{2 - \max - \min}, \quad \text{if } L > 0.5, \tag{2b}$$

$$H = 0, \quad \text{if } S = 0, \tag{3a}$$

$$H = 60 \cdot \frac{(G - B)}{\max - \min}, \quad \text{if } \max = R, \tag{3b}$$

$$H = 60 \cdot \left[2 + \frac{(B - R)}{\max - \min}\right], \quad \text{if } \max = G, \tag{3c}$$

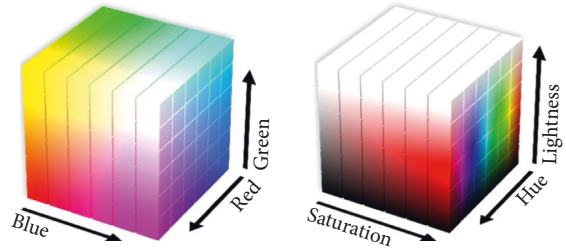

(a) (b)

Figure 2: Cubic interpretation of RGB (a) and HSL (b) models.

$$H = 60 \cdot \left[4 + \frac{R - G}{\max - \min}\right], \quad \text{if } \max = B. \tag{3d}$$

2.3. Rheological Analysis. The main rheological properties of the studied binders were then assessed through a Dynamic Shear Rheometer (DSR). According to EN 14770, the rheological tests were carried out using plate-plate geometry with 25.00 mm diameter plate and 1.00 mm gap or 8.00 mm diameter plate and 2.00 mm gap depending on the test temperature. A conditioning period of at least 15 minutes was fixed for each testing temperature, in order to guarantee a homogeneous thermal distribution within the specimens.

First, strain sweep tests were performed to identify the linear viscoelastic (LVE) domain at the different test temperatures and frequencies. The LVE limit of studied materials was established in correspondence of the decrease to 95% of the initial complex modulus G^* [22, 23]. This was accomplished by performing amplitude sweep (AS) oscillatory tests at the standard angular frequency ω of 10 rad/s (1.59 Hz) and in the range of temperature from 10 to 50°C (with 10°C steps), recording the evolution of G^* as a function of the strain amplitude γ (varied from 0.01% to 100% as represented in Figure 3(a)). Two test replicates were carried out for each test condition.

Then, oscillatory temperature sweep (TS) tests were carried out to detect the temperature dependency of the studied materials. The experimental results were plotted in terms of isochronal curves of the storage modulus G' (i.e., the elastic component of the complex modulus) and the loss modulus G'' (i.e., the viscous component of the complex modulus) as a function of the test temperature (T). In this case, the binders were subjected to strain-controlled oscillatory tests applying a constant amplitude within the LVE domains ($\gamma = 0.05\%$) and using the 8 mm parallel plate geometry at a constant ω of 10 rad/s (1.59 Hz). During this test, the temperature was increased linearly from 4 to 76°C (Figure 3(b)). Three test replicates were carried out for each test condition.

Frequency sweep (FS) tests were then executed in oscillatory strain-controlled loading conditions (within the LVE domain), varying the frequency from 100 to 0.1 rad/s (ramp log decreased with a slope of 10 points/decade) and adopting a range of temperatures between 4 and 76°C, with steps of 6°C. In particular, 8 and 25 mm diameter parallel plates were selected for tests between 4°C and 34°C and between 34 and 76°C, respectively. All tested samples were previously subjected to PAV procedure to simulate the long-term aging, i.e., the worst conditions for midservice temperature cracking resistance. Frequency sweeps allow the construction of the master curves by using the well-knownTime-Temperature Superposition Principle (TTSP), generally valid for thermorheologically simple materials (e.g., traditional bitumens). In this case, a single smooth master curve of the selected LVE characteristics (e.g., G^*) is obtained by shifting the experimental data series with horizontal shift factors a_T related to test frequency (or time) and vertical shift factors b_T proportional to the material density. In this regard, frequency sweep test results were elaborated to construct master curves both for the complex modulus G^* and the phase angle δ at the reference temperature T_0 of 34°C. To this aim, the reduced angular frequency ω_r is defined in the following equation:

$$\omega_r(T_0) = a_T \cdot \omega(T), \tag{4}$$

where ω indicates a generic experimental frequency. The horizontal shift factors a_T were chosen to fit with the Williams–Landel–Ferry (WLF) formulation [24]:

$$\log a_T = -\frac{C_1 \cdot (T - T_0)}{C_2 + (T - T_0)}, \tag{5}$$

where C_1 and C_2 represent empirical material constants related to the free volume and its thermal expansion coefficient. Despite the specific elaboration used for bituminous materials, vertical shifting is also possible. It could be realized with b_T vertical factors according to the following equation:

$$T_0 \cdot \rho_0 = b_T \cdot T \cdot \rho, \tag{6}$$

where ρ is the material density at the given temperature T and ρ_0 is the density at the reference temperature T_0. Due to the synthetic nature of the studied resin, a tentative vertical shifting was also applied.

The fatigue resistance of the studied binders was also investigated through the linear amplitude sweep (LAS) test which consists of a time-saving and effective (especially for comparative purposes) laboratory procedure to obtain the fatigue law of a bituminous binder with respect to the traditional time sweep analysis, i.e., a series of oscillatory shear tests at a selected frequency and different constant strain amplitudes [25–28]. According to AASHTO TP 101-14, LAS tests were performed on 8 mm diameter specimens by

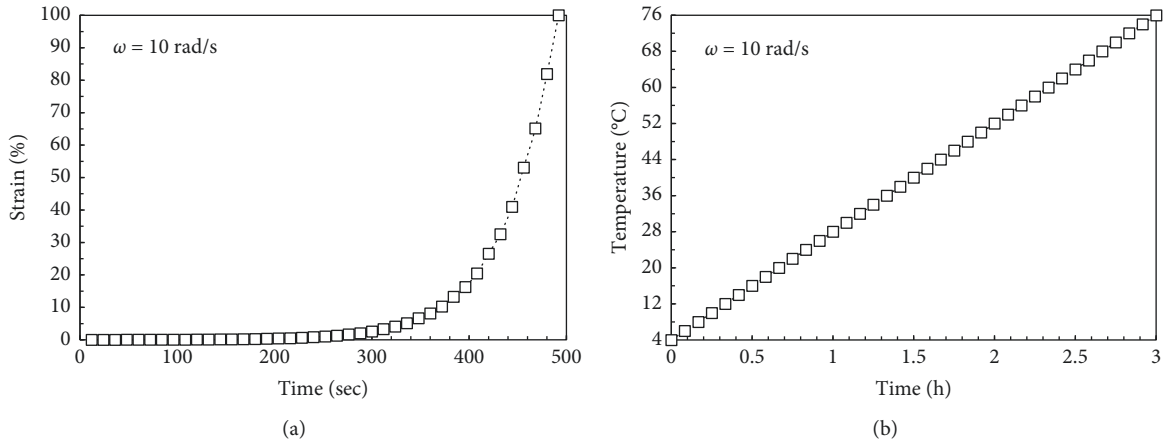

Figure 3: Preliminary test configuration: amplitude sweep (a) and temperature sweep (b) tests.

performing a two-phase test protocol, consisting of a preliminary frequency sweep followed by a series of amplitude sweeps progressively increasing the strain amplitude to cause accelerated fatigue damage [29]. In particular, the frequency sweep was carried out by applying an oscillatory strain having a constant amplitude of 0.1% over a frequency interval ranging from 0.2 to 30 Hz (linear continuous ramp depicted in Figure 4(a)). Then, the following amplitude sweeps were performed at the constant frequency of 10 Hz, linearly increasing the strain from 0 to 30% over 3,100 loading cycles (Figure 4(b)) and recording G^* and δ values. LAS test temperature was fixed at 20°C. Three replicates for each material were carried out.

The fatigue law of the tested materials (i.e., the cycles to fatigue failure N_f as a function of the strain amplitude γ) was defined based on (i) the determination of undamaged material properties (α parameter) from the frequency sweep phase; (ii) the viscoelastic continuum damage (VECD) analysis from the amplitude sweep phase (based on the VECD theory) [29]. Despite some literature ambiguity about the first-undamaged phase [30, 31], α was calculated according to standard specifications:

$$\alpha = \frac{1}{m}, \tag{7}$$

where m represents the slope of the regression line applied to the first-phase bilogarithmic plot reporting G' as a function of ω:

$$\log G' = m \cdot (\log \omega) + b, \tag{8}$$

where b is the curve intercept. Assuming $C(t)$ as the material integrity (i.e., the ratio of G^* at a given time t to the initial G^*) and γ as the related applied strain amplitude (in percent), the damage $D(t)$ accumulated during the second phase of test (amplitude sweep) was calculated according to the following equation:

$$D(t) = \sum_{i=1}^{N} \left[\pi \cdot \gamma^2 \cdot \left(C_{i-1} - C_i\right)\right]^{\alpha/(1+\alpha)} \cdot \left(t_i - t_{i-1}\right)^{1/(1+\alpha)}, \tag{9}$$

where i indicates the given loading step. Figure 5(a) represents a typical $C(t)$ vs. $D(t)$ plot. The logarithmic plot of $C_0 - C(t)$ vs. $D(t)$ (i.e., integrity loss vs. damage) represented in Figure 5(b) allowed the determination of the fitting coefficients C_1 and C_2 (C_0 was assumed equal to 1 according to AASHTO TP 101-14).

Thus, the fatigue law reported in equation (10) can be calculated as follows:

$$N_f = A \cdot \gamma^{-B}, \tag{10}$$

$$A = \frac{f \cdot \left(D_f\right)^{1+\left(1-C_2\right)\cdot\alpha}}{\left(1 + \left(1 - C_2\right)\cdot\alpha\right)\left(\pi \cdot C_1 \cdot C_2\right)^{\alpha}}, \tag{11}$$

$$B = 2 \cdot \alpha, \tag{12}$$

where f is the test frequency (10 Hz), whereas D_f indicates the damage value at sample failure as defined in the following equation:

$$D_f = \left[\frac{C_0 - C_{\text{at Peak Stress}}}{C_1}\right]^{1/C_2}. \tag{13}$$

Finally, Multiple Stress Creep Recovery (MSCR) tests were performed in order to evaluate the rutting potential of the studied binders at high-service temperatures. According to EN 16659, the test consists of ten creep-recovery cycles (1 s constant loading and 9 s unloading) carried out at two different consecutive stress levels (0.1 and 3.2 kPa). In particular, temperature and stress dependencies were evaluated on RTFO-aged materials (worst condition for rutting potential) using 25 mm diameter samples at temperatures of 52, 58, 64, 70, and 76°C. Three test replicates were carried out for each material and test condition.

The rutting potential was then assessed by representing the strain evolution over time and calculating the nonrecoverable creep compliance (J_{nr}) as well as the J_{nr}/J_{TOT} ratio. J_{nr} and J_{nr}/J_{TOT} formulations are described in equations (14) and (15), respectively:

$$J_{nr}^n = \frac{\varepsilon_r^n - \varepsilon_0^n}{\tau^n}, \tag{14}$$

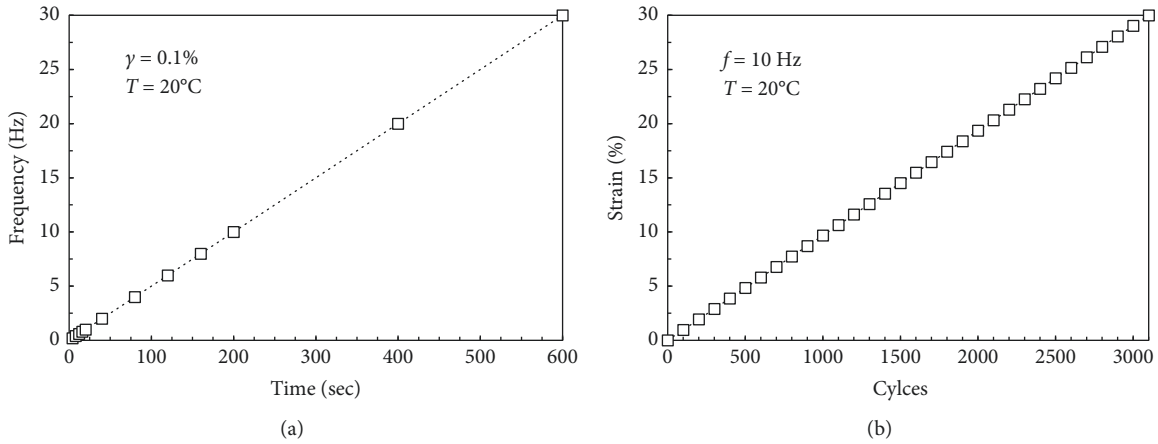

Figure 4: LAS test: 1st phase frequency sweep (a) and 2nd phase amplitude sweep (b).

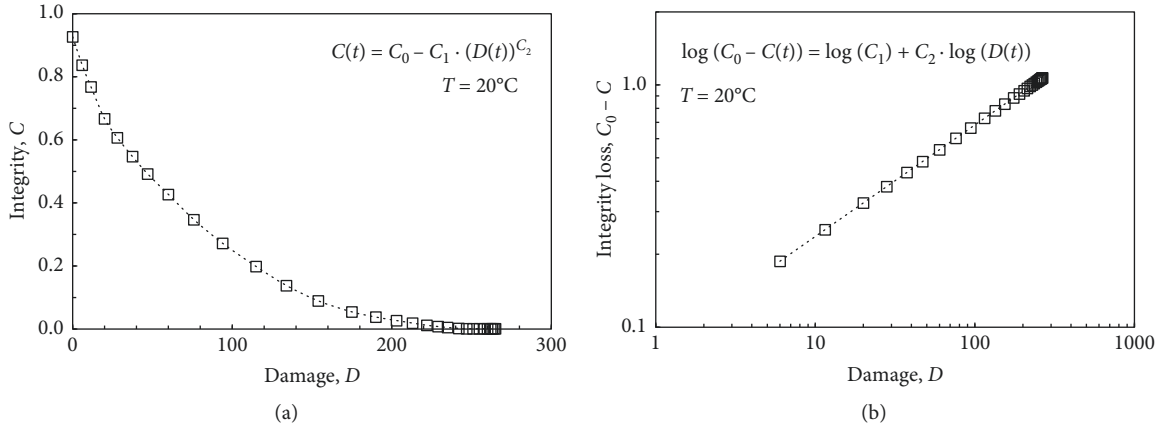

Figure 5: Typical LAS test results: integrity vs. damage (a); integrity loss vs. damage (b).

$$\frac{J_{\text{nr}}}{J_{\text{TOT}}} = \frac{(\varepsilon_r^n - \varepsilon_0^n)/\tau^n}{(\varepsilon_c^n - \varepsilon_0^n)/\tau^n} = \frac{\varepsilon_r^n - \varepsilon_0^n}{\varepsilon_c^n - \varepsilon_0^n}, \tag{15}$$

where n indicates the cycle number, τ the applied stress at the n-cycle, ε_r^n the final strain after the entire n-cycle (10 s), ε_0^n the strain at the beginning of n-cycle, and ε_c^n the strain at the end of the creep phase (1 s) at the n-cycle.

As it can be noted, J_{nr} refers only to the nonrecovered (i.e., plastic) strains at the end of each cycle, whereas $J_{\text{nr}}/J_{\text{TOT}}$ normalizes J_{nr} with respect to the creep compliance at the end of creep phase (corresponding to the maximum measured strain ε_c). For each sample, the average J_{nr} and $J_{\text{nr}}/J_{\text{TOT}}$ for each stress magnitude are then calculated.

As a summary, Figure 6 schematizes the overall experimental plan of the proposed research.

3. Results and Discussion

3.1. Chromatic Results. The chromatic test results are summarized in Table 2, whereas Figures 7 and 8 report an example of the captured images of the samples and the visual representation of the corresponding chromatic HSL properties, respectively.

As expected, the tested bitumen demonstrated a deeply dark aspect, almost close to the pure black colour, whereas the synthetic binder showed completely different chromatic characteristics. As far as the influence of the aging process on the CSR colour is concerned, it can be noted that the tonalities of the three samples (unaged, RTFO-aged, and PAV-aged) were similar at the different aging conditions. In particular, H coordinates exhibited only slight variations due to aging, whereas the saturation S seemed more affected by the aging processes, changing from 34% (unaged resin) to 98% and 99% in aged conditions. Analogous considerations could be extended to lightness (L) values, which moved from 47% in the unaged condition to 35–38% for the aged samples, with a minor difference between RTFO-aged and PAV-aged CSR. Thus, it could be stated that the colour of virgin CSR product did not exactly correspond to that of the material after the paving operations (simulated by RTFO laboratory procedure), whereas long-term aging effects on the CSR colour (simulated by PAV laboratory procedure) should be considered nearly negligible. However, it is worth noting that the colour of the pavement surface over its service life is strongly affected by the colour of the aggregates used (in particular when a clear binder is used) and also due

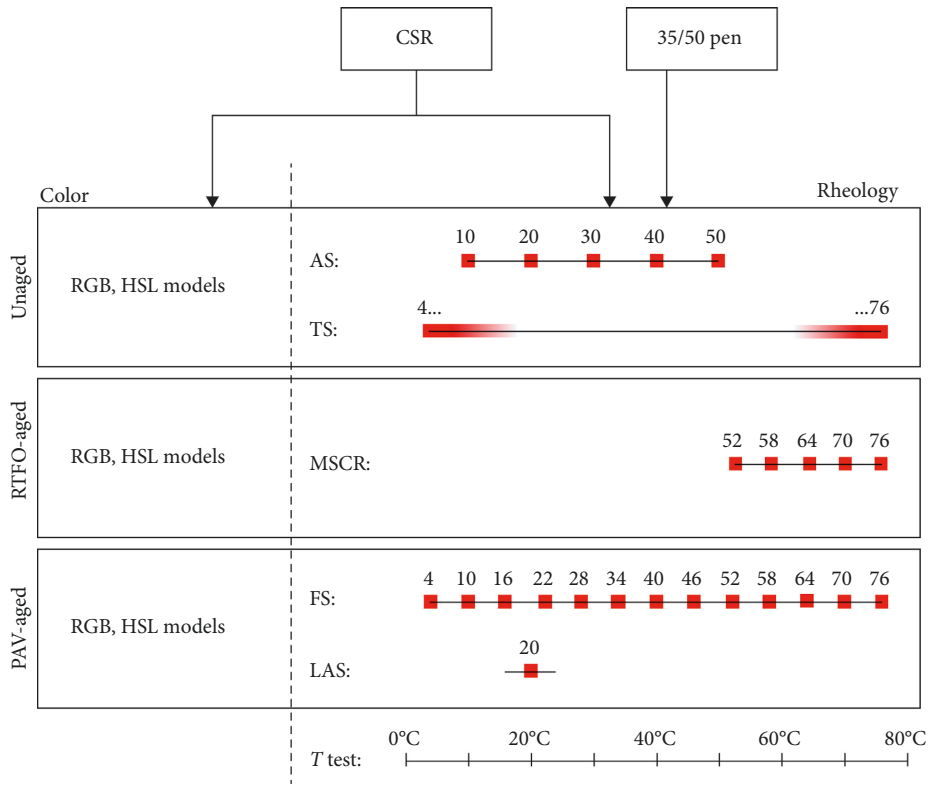

Figure 6: Summary of the experimental plan.

Table 2: Summary of chromatic test results.

Material	Colour model					
	RGB			HSL		
	R	G	B	H (°)	S (%)	L (%)
35/50 pen	1	4	2	140	60	1
CSR (unaged)	200	130	38	34	68	47
CSR (RTFO-aged)	193	114	2	35	98	38
CSR (PAV-aged)	177	76	1	26	99	35

to other "external" factors such as the interactions with vehicle tires, spillages (fuel, oil, etc.), and "environmental" dirt. A specific research study addressing the above-mentioned aspects is already planned.

3.2. Rheological Results. Amplitude sweep (AS) tests were preliminarily carried out in order to investigate the strain-dependency of the studied materials and to identify their linear viscoelastic domains. Average experimental data collected during the AS tests are depicted in Figures 9 and 10 and summarized in Table 3.

Both the traditional bitumen (Figure 9) and the CSR resin (Figure 10) exhibited the typical behaviour represented by a G^* not dependent on the strain level until the corresponding LVE limit, after which a rapid decrease of the complex modulus occurred highlighting the nonlinear viscoelastic domain. Comparing 35/50 pen and CSR binders, it can be observed that the reference bitumen is evidently stiffer than the clear resin at low temperatures, whereas this difference progressively decreased with the increase of the test temperature (CSR and the traditional bitumen showed comparable G^* values at 50°C) denoting a lower temperature-dependence of CSR. Overall, the LVE strain limits reported in Table 3 showed a conventional proportional relation with the measured G^* for both 35/50 pen and CSR binders [32].

Figure 11 reports the temperature sweep oscillatory test results in terms of storage G' and loss G'' moduli as a function of the test temperature in order to highlight the temperature dependencies of the studied materials.

Overall, reduced slopes of CSR curves were well recognized, thus indicating a lower temperature susceptibility of the studied resin with respect to the reference bitumen; this is also in accordance with the basic characteristics reported in Table 1 and already discussed. Similarly to what was arising from the preliminary amplitude sweep test results, the synthetic resin revealed to be softer than the 35/50 penetration grade bitumen at the lower temperatures, whereas both G' and G'' of CSR seemed to be equivalent (or even slightly higher) at the highest analysed temperatures with respect to the corresponding characteristics of the reference bitumen. This could represent a promising finding both for low-temperature cracking phenomenon and mid-temperature fatigue resistance without a clear reduction of the rutting resistance at higher temperatures. However, a lower structural contribution of the CSR-based mixtures can be hypothesized due to its reduced G^*. Some of these aspects are specifically addressed in the following. Moreover, it is worth noting that the 35/50 pen bitumen was characterized by a predominant viscous behaviour at a temperature higher

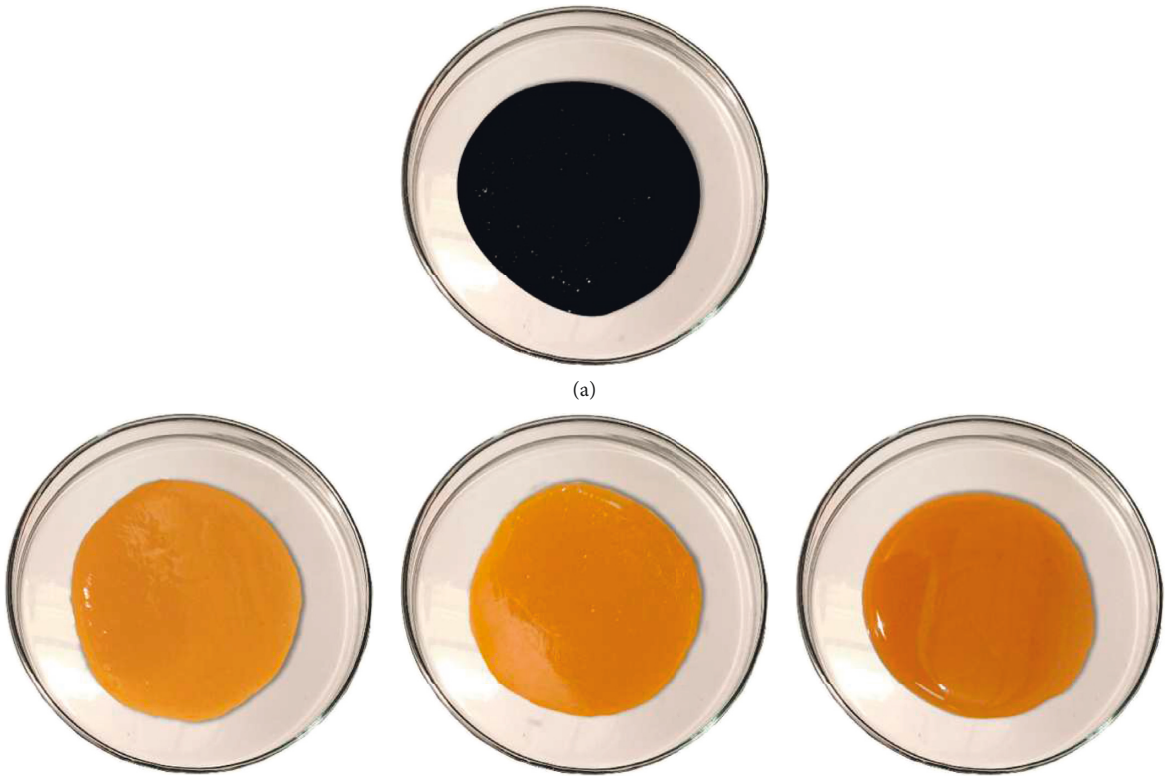

(a) (b) (c) (d)

Figure 7: Acquired pictures: bitumen (a); unaged CSR (b); RTFO-aged CSR (c); PAV-aged CSR (d).

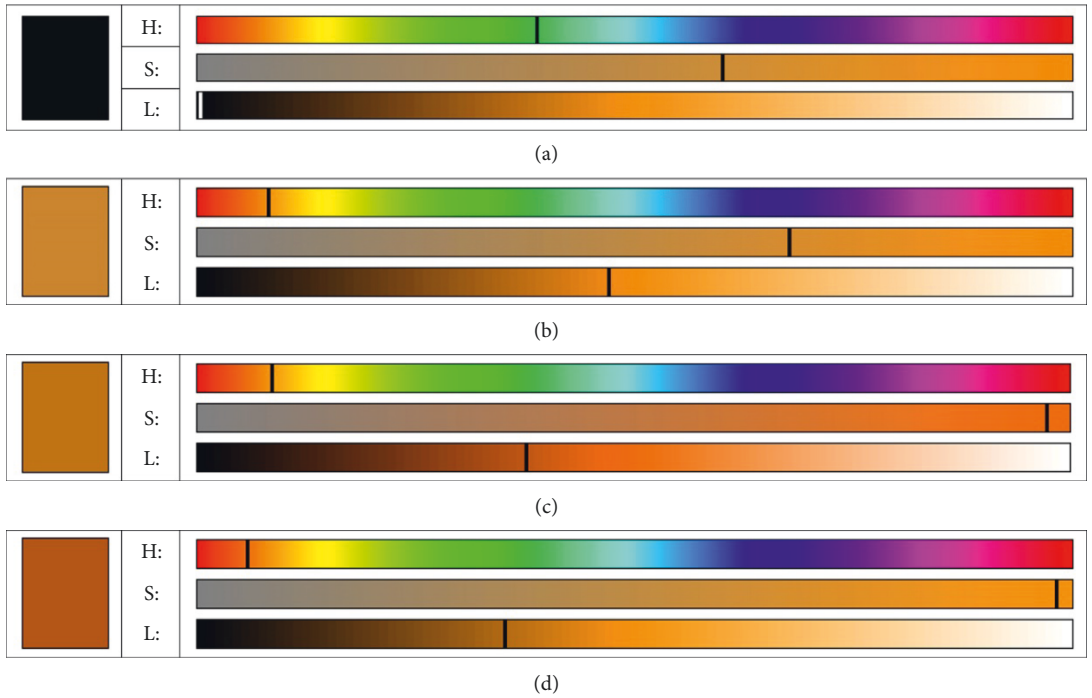

Figure 8: HSL colour model results: bitumen (a); unaged CSR (b); RTFO-aged CSR (c); PAV-aged CSR (d).

than 20°C (G'' significantly higher than G'), whereas CSR showed very similar values of G' and G'' at all the tested temperatures, being G'' only slightly higher than G'.

The main linear viscoelastic response of the tested materials is discussed below through the frequency sweep test results. The validity of TTSP for the tested materials was

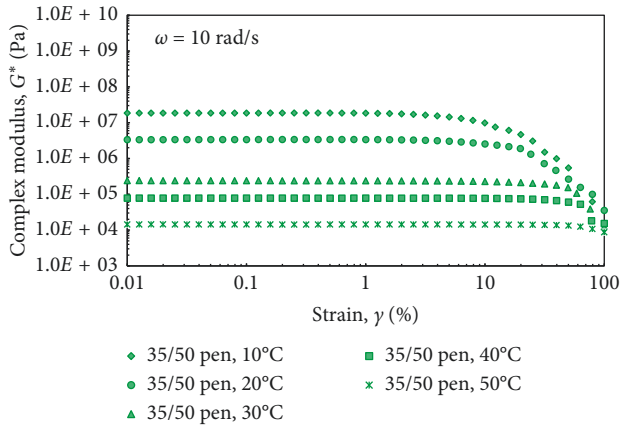

Figure 9: Amplitude sweep experimental test results (G^* vs. γ)—35/50 pen.

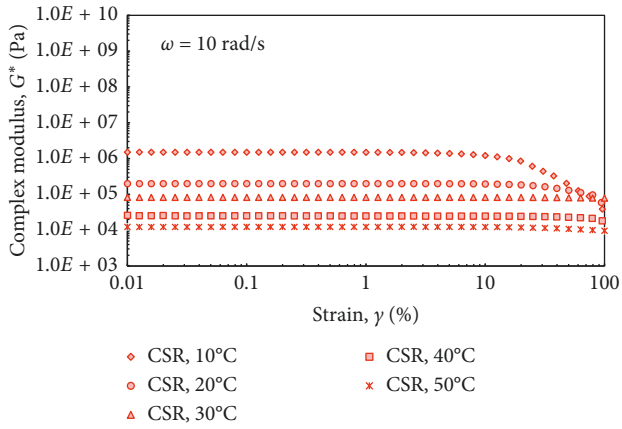

Figure 10: Amplitude sweep experimental test results (G^* vs. γ)—CSR.

Table 3: Summary of amplitude sweep test results: initial G^* and LVE limit.

Temperature (°C)	35/50 pen		CSR	
	Initial G^* (Pa)	LVE limit (%)	Initial G^* (Pa)	LVE limit (%)
10	18 556 338	1.82	1 507 503	3.57
20	3 358 052	3.47	200 186	15.96
30	241 327	8.21	82 764	32.82
40	78 802	18.97	26 111	37.61
50	14 439	42.55	10 595	45.73

preliminarily checked by analysing the measured complex moduli and phase angles in the Black space (δ vs. G^* plot), since it is ascertained that smooth curves in this space indicate the validity of such a superposition principle [14, 33] avoiding inconsistent data fitting with horizontal and vertical shifting. Given this background, the 35/50 pen bitumen exhibited a practically smooth trend in the Black space (Figure 12), thus allowing the consistent construction of G^* master curve (Figure 13) and δ master curve (Figure 14) at the reference temperature of 34°C. It can be noted that the complex shear modulus (Figure 13) smoothly increased with

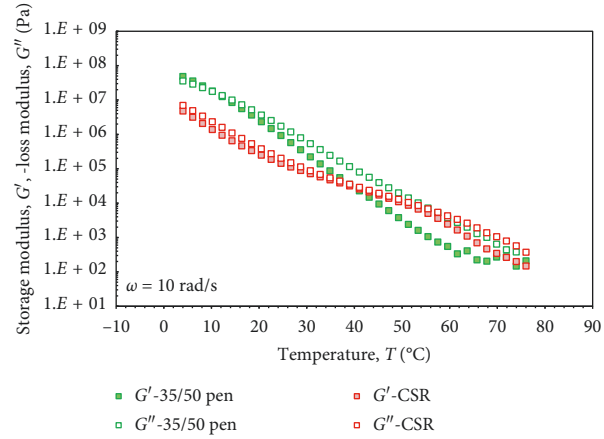

Figure 11: Temperature sweep test results at 10 rad/s: G', G'' vs. T (35/50 pen and CSR).

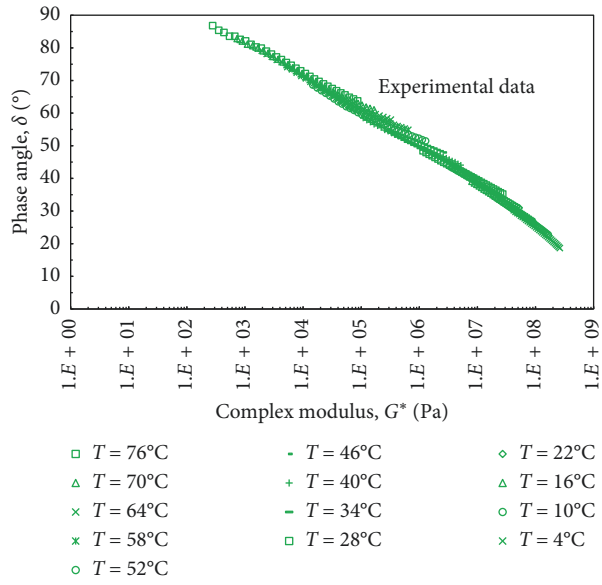

Figure 12: Black diagram (δ vs. G^*)—35/50 pen.

the test frequency and seemed to approach the glassy asymptote ($G^* = 10^9$ Pa) at the lower tested temperature and highest frequency. On the other hand, the measured phase angle increased with the test temperature (thus decreasing the reduced frequency) achieving values of about 80°. In the tested temperature range, a prevalent elastic behaviour ($\delta < 45°$) was guaranteed up to $28 \div 40$°C, depending on the corresponding test frequency.

The measured G^* and δ of the CSR resin are shown in the Black space of Figure 15. In this case, the experimental data did not provide a smooth curve, indicating the partial inconsistency of the TTSP, at least for the analysed temperatures and frequencies. Therefore, the construction of G^* and δ master curves for CSR was not possible. In any case, different behaviours seemed to be recognizable depending on the test temperatures. This experimental finding could be rationally explained considering the bicomponent nature of the tested resin and the fact that the melting processes could cause the discontinuity and the transition since different

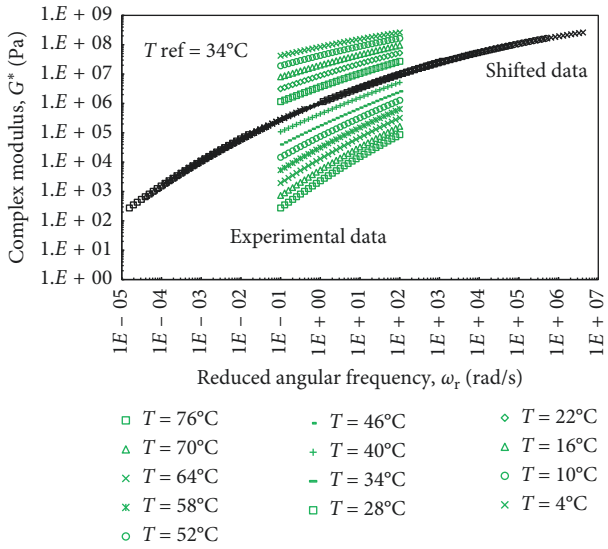

Figure 13: Complex modulus master curve (G^* vs. ω_r)—35/50 pen.

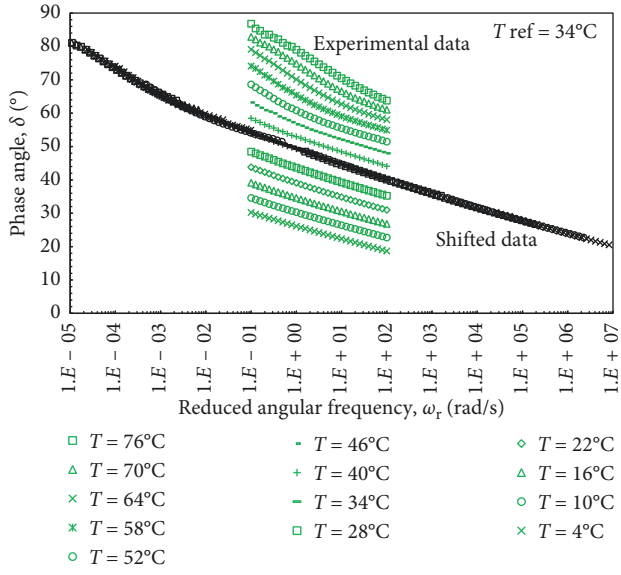

Figure 14: Phase angle master curve (δ vs. ω_r)—35/50 pen.

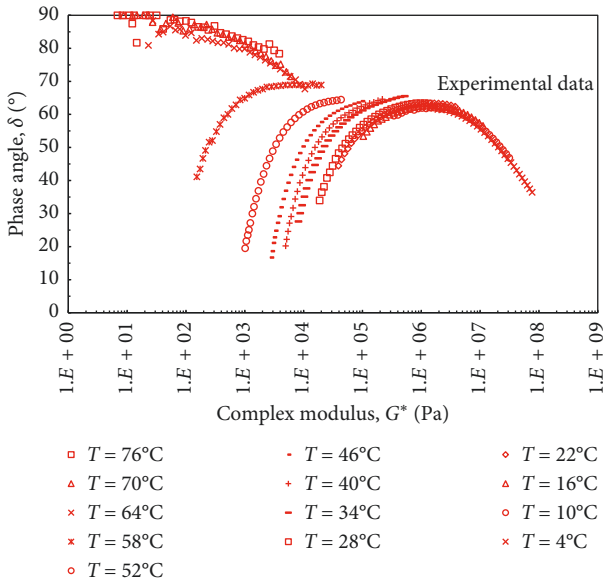

Figure 15: Black diagram (δ vs. G^*)—CSR.

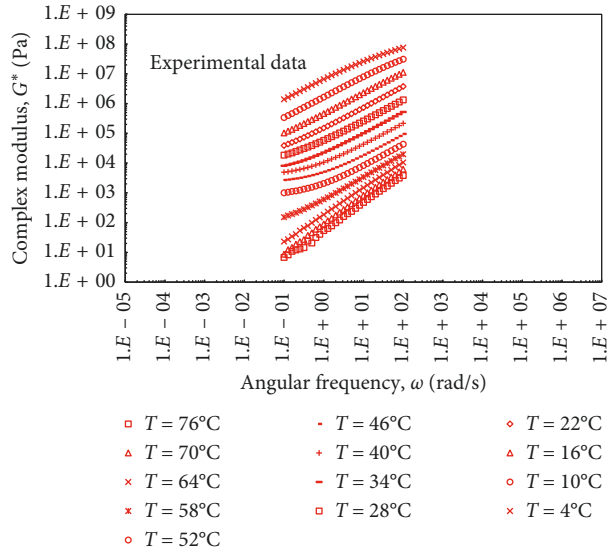

Figure 16: Experimental results of complex shear modulus (G^* vs. ω)—CSR.

compounds reasonably conferred distinct properties to the synthetic binder. Moreover, it is interesting to note the unconventional "bell-shape" of the data series measured at temperatures up to 58°C for which δ initially increased with G^* (opposite trend with respect to that of traditional bitumens) and then started to decrease. In this sense, the overall distribution of the measured LVE characteristics seemed to indicate the existence of three distinct regions, as discussed in detail below.

Figure 16 plots CSR complex modulus experimental data showing that G^* increased with increasing test frequencies and decreasing test temperatures, according to a typical viscous thermoplastic behaviour of bituminous binders. However, at the lowest and the highest investigated temperatures, CSR exhibited conventional quasilinear trends (similar to those of traditional bituminous binders), whereas at intermediate temperatures (approximately between 22 and 58°C), G^* revealed unusual s-shaped curves, flattened in the proximity of the lowest experimental ω.

As far as the phase angle δ is concerned (Figure 17), a nonconventional behaviour (i.e., different from that of bitumens) was observed in the tested range of temperatures and frequencies, distinguishing the three abovementioned different trends which can be broadly schematized as (i) from 4 to 16°C, phase angles decreased as the frequency increased; (ii) from 16 to 58°C, a transition towards the opposite tendency can be detected (δ increasing with frequency); and (iii) from 58 to 76°C, a further clear change of behaviour occurred towards a trend similar to that observed for the lowest temperatures (δ decreasing as the frequency increases).

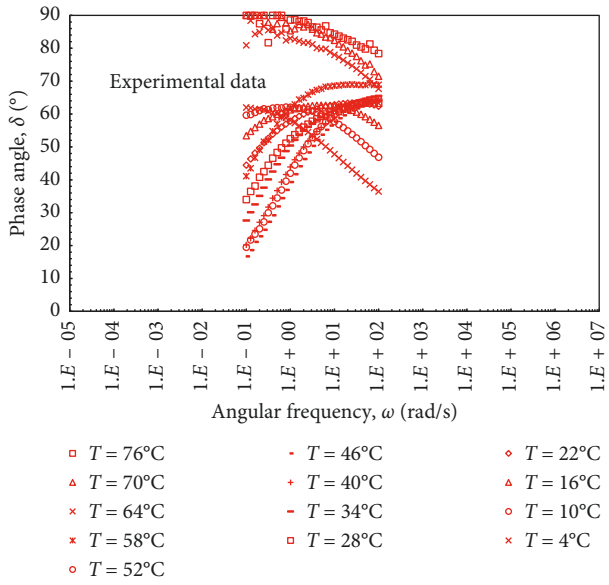

FIGURE 17: Experimental results of phase angle (δ vs. ω)—CSR.

The comparison of the linear viscoelastic properties of the tested binders is reported in the following, based on the trend of the measured experimental data G^* and δ (Figures 18 and 19). Overall, the resin showed significantly lower stiffness than the traditional bitumen at a given temperature within the investigated frequency domain (Figure 18). As an example, complex modulus of the bitumen at 52°C was comparable with G^* at 28°C of the resin at a given test frequency.

Moreover, CSR exhibited noticeably higher δ at both low ($4 \div 22$°C) and high ($64 \div 76$°C) test temperatures (even approaching 90° corresponding to a pure viscous behaviour) than the 35/50 pen bitumen, thus denoting a more viscous behaviour in that domain (Figure 19). On the other hand, given the observed properties of CSR discussed above, a direct comparison between the two binders at intermediate temperatures ($22 \div 58$°C) is not straightforward. However, with the aim of finding a correlation between these data and the empirical findings related to the elastic recovery of the materials measured at 25°C (Table 1), phase angle values at $22 \div 28$°C and low frequencies can be compared. In this sense, a certain correlation could be observed since CSR seemed to exhibit lower phase angles at these test conditions than the traditional bitumen, thus denoting higher elasticity. Specific considerations related to fatigue resistance at intermediate temperatures and rutting potential at high-temperatures are given in the following, based on the corresponding specific rheological tests carried out.

The fatigue resistance of CSR and reference 35/50 pen bitumen assessed by LAS tests is summarized in Table 4 and Figure 20, which report the main LAS outcomes and the corresponding predicted fatigue lines, respectively.

First of all, the soundness of the obtained results seems to be confirmed by the fact that they are in accordance with those of previous studies on traditional bitumens [30]. The derived fatigue curves (Figure 20) indicated a significant

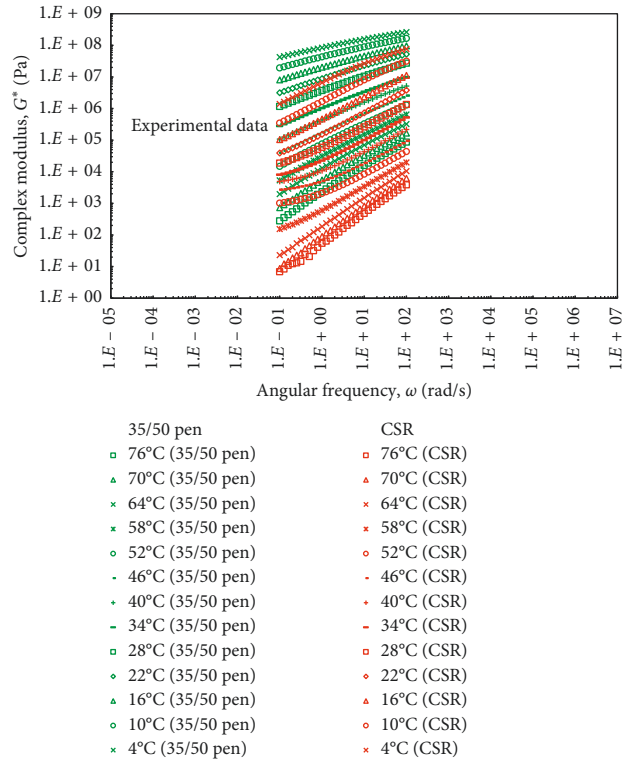

FIGURE 18: Experimental results of stiffness (G^* vs. ω)—35/50 pen vs. CSR.

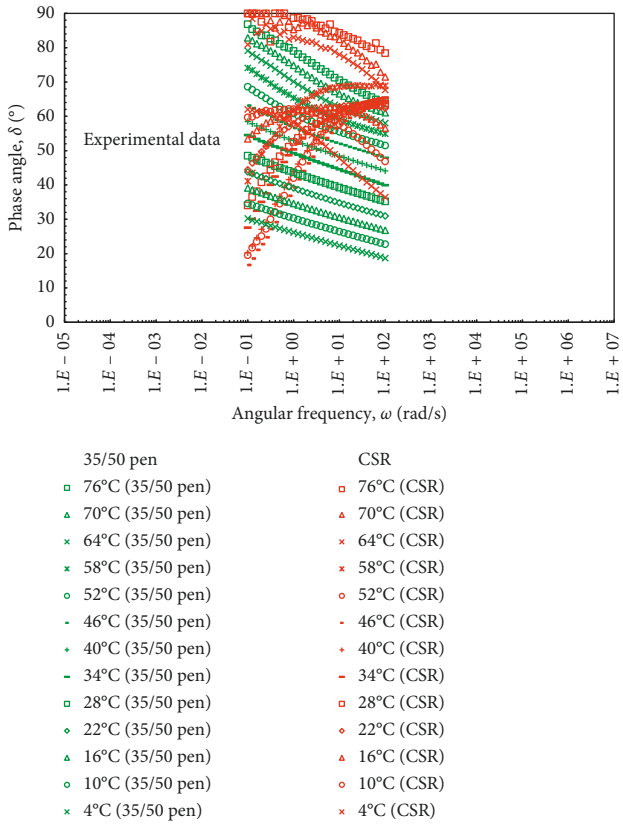

FIGURE 19: Experimental results of phase angle (δ vs. ω)—35/50 pen vs. CSR.

Table 4: Linear amplitude sweep parameters.

Material	LAS parameter						
	M	α	C_1	C_2	D_f	A	B
35/50 pen	0.6749	1.4817	0.0872	0.5624	14.5167	7970.07	2.963
CSR	0.7681	1.3019	0.0365	0.6264	45.4842	60419.17	2.604

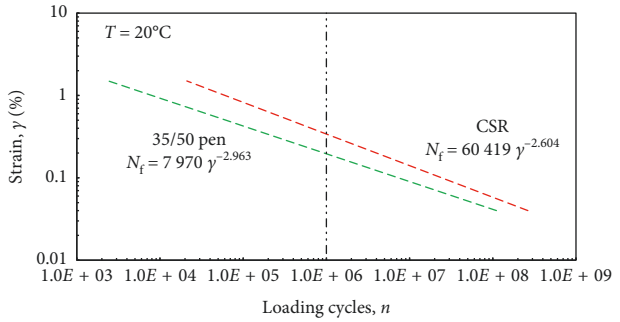

Figure 20: LAS test results (γ vs. n)—35/50 pen vs. CSR predicted fatigue lines.

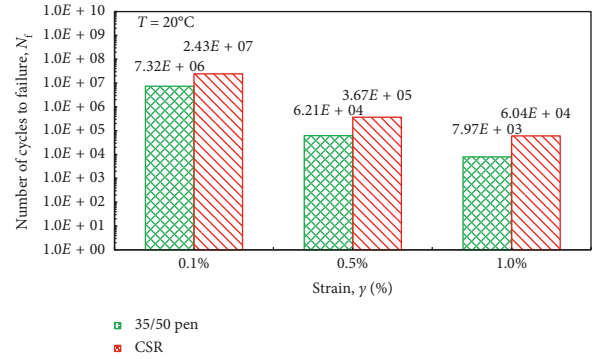

Figure 21: LAS test results (N_f vs. γ)—35/50 pen vs. CSR loading cycles at failure.

improvement of the fatigue resistance in the case of CSR binder. In this respect, Figure 21 details the increase of number of cycles to failure for CSR at some representative strain levels (0.1, 0.5, and 1.0%) based on the above-mentioned fatigue lines. These findings seem to agree with the main linear viscoelastic rheological properties discussed in the previous sections where it was highlighted a reduced stiffness of CSR at the intermediate temperatures (LAS tests were carried out at 20°C), which should lead to a higher ductility of such a synthetic binder and thus to reduced cracking phenomenon. In this case, the lower stiffness of CSR (at 20°C) led to lower shear stress at fixed strain levels (Figure 22) up to τ peak value of the 35/50 pen bitumen, which corresponds to the sample failure, as well as to a noticeably higher damage at failure D_f achieved by CSR (Table 4). Thus, faster G^* reduction and greater damage accumulation for 35/50 pen were reasonably possible.

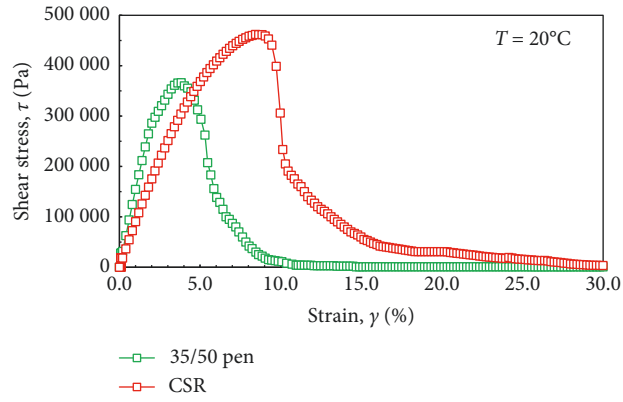

Figure 22: LAS test results (τ vs. γ)—35/50 pen vs. CSR shear stress evolution.

As far as permanent deformation resistance is concerned, MSCR test results are presented in Figure 23 where the experimental data collected for both the tested binders are reported in terms of strain evolution over time. First, a strong temperature dependency could be clearly evinced in the case of CSR resin since the measured strains exhibited a very fast increase as the test temperature increased thus confirming the LVE properties presented above. In particular, CSR and 35/50 pen showed a comparable behaviour at 52°C and 58°C (CSR permanent deformation resistance at 52°C seemed even higher than that of the traditional bitumen) whereas sensibly higher strains were measured for CSR samples at the higher analysed temperatures (64, 70 and 76°C).

J_{nr}/J_{TOT} and J_{nr} values calculated based on the experimental readings depicted in Figure 23 are summarized in Table 5 and represented in Figure 24, respectively. First, the results of Table 5 and Figure 24 clearly highlight the different stress and temperature dependency of the two

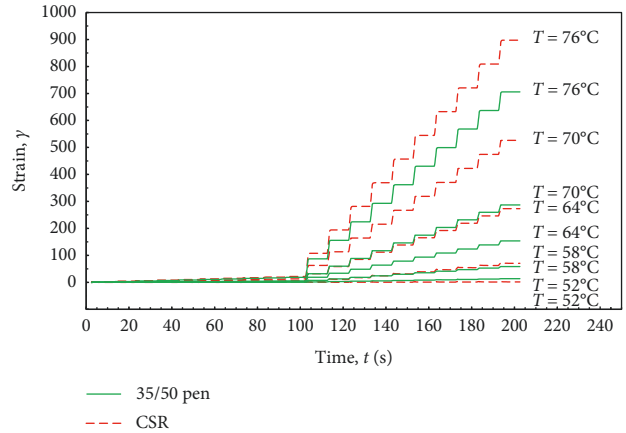

Figure 23: MSCR test results (γ vs. t)—35/50 pen vs. CSR strain evolution.

Table 5: MSCR test results—J_{nr}/J_{TOT} ratios.

Temperature (°C)	J_{nr}/J_{TOT} ratio			
	35/50 pen		CSR	
	$\tau = 0.1$ kPa	$\tau = 3.2$ kPa	$\tau = 0.1$ kPa	$\tau = 3.2$ kPa
52	0.88	0.91	0.02	0.08
58	0.95	0.98	0.12	0.77
64	0.98	1.00	0.87	0.99
70	0.99	1.00	0.94	1.00
76	0.99	1.00	0.98	1.00

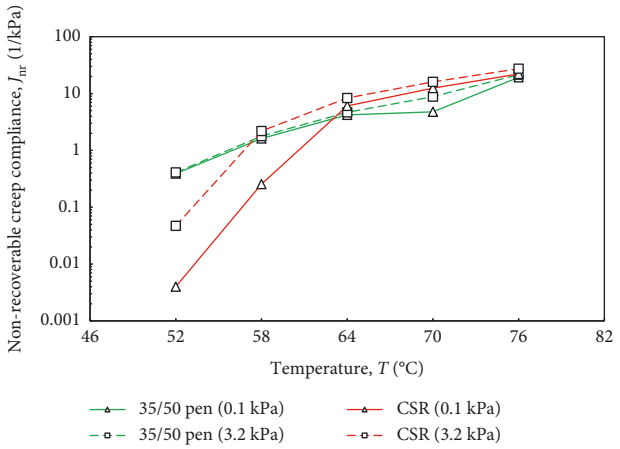

Figure 24: MSCR test results (J_{nr} vs. T)—35/50 pen vs. CSR nonrecoverable creep compliance.

materials up to 64°C. In particular, such results clearly show the noticeable elastic recovery aptitude of CSR, especially for temperatures up to 58°C. On the other hand, some issues occurred for CSR at the higher temperatures in terms of nonrecoverable creep compliance J_{nr}, which takes into account the permanent deformation at the end of the creep phase in relation with the corresponding applied stress level. This finding seems in accordance with the frequency sweeps results reported in the Black space of Figure 15, which denoted this specific temperature dependency (a clear change in behaviour was observed moving from 58 to 64°C).

However, it is worth highlighting that, at given environmental conditions (air temperature, solar radiation, humidity, wind, etc.), clear mixtures will achieve distinctly lower in-service temperatures than traditional "black" materials due to their chromatic and thermal properties [34]. Thus, a proper comparison between the two tested binders regarding their rutting resistance at high-temperatures should be carried out taking into account the different temperatures that clear and traditional materials would achieve in the field. As an example, Figures 25 and 26 represent a plausible scenario demonstrating that, if a surface course prepared with CSR will achieve in the field a temperature 6°C lower than that of a corresponding reference bituminous mixture (thanks to its chromatic and thermal properties), it will be able to guarantee distinctly higher performance in terms of permanent deformation resistance than that of traditional materials, thus demonstrating promising applicability.

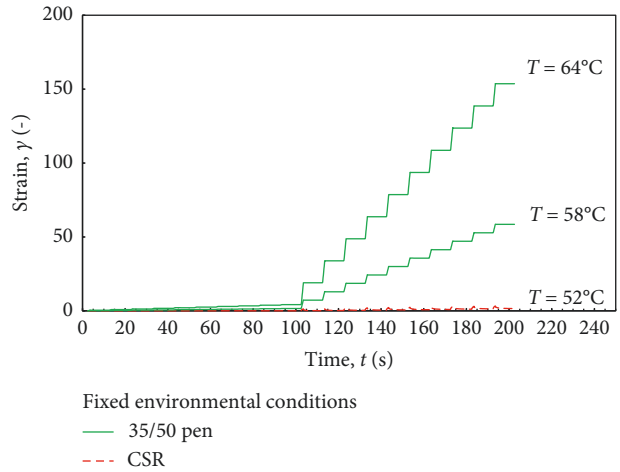

Figure 25: Hypothesis scenario (γ vs. t)—35/50 pen vs. CSR strain evolutions at different temperatures.

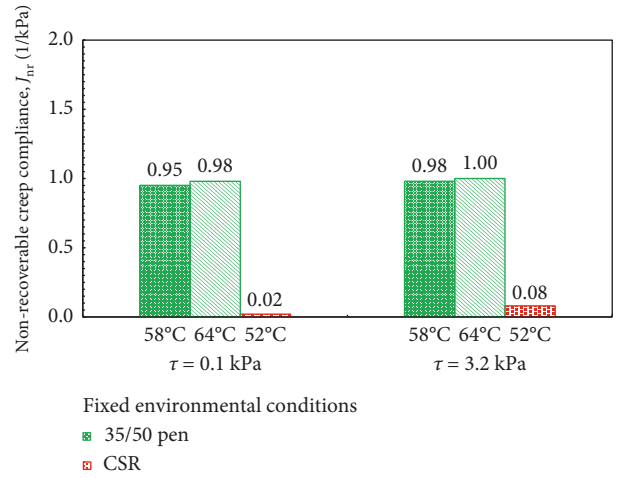

Figure 26: Hypothesis scenario (J_{nr})—35/50 pen vs. CSR J_{nr} at different temperatures.

4. Conclusions

The present paper deals with an experimental study aimed at assessing aesthetic and rheological properties of a synthetic transparent resin (CSR) for clear road pavement surface courses. The observed performance was also related with that of a conventional 35/50 penetration grade bitumen (35/50 pen) selected as a reference binder for comparison purposes.

The chromatic analysis was performed to determine objective parameters describing the visual appearance of the resin and to investigate the aging effects on such chromatic characteristics, also in view of subsequent analysis aimed at quantifying correlation between colour and thermal properties. The chromatic characteristics of the tested materials were evaluated through hue, saturation, and lightness model. The experimental findings mainly revealed that

(i) hue (i.e., tonality) of CSR did not seem to be significantly affected by aging

(ii) saturation (i.e., light emission power) and lightness (i.e., colour brightness) showed higher variations due to aging (mainly related to the short-term aging)

Thus, a good chromatic durability of mixtures prepared with CSR could be supposed (once paved, binder colour should be affected by weathering and oxidizing to a limited extent). Indeed, a chromatic assessment at mixture scale is strongly suggested in order to both consider the possible in-service issues related to the pavement dirtying (vehicle tire actions, spillages, and atmospheric agents) and to determine the influence of aggregate colour in the final tonality of the mix (i.e., the transparency of the resin should exalt the chromaticity of the lithic matrix).

A comprehensive rheological characterization was also carried out to determine the main linear viscoelastic characteristics, the fatigue resistance, and the rutting potential of the investigated binder. In this sense, the obtained results mainly suggested that the clear synthetic resin

(i) cannot be considered a thermorheologically simple material (time-temperature superposition principle not valid)

(ii) seemed to be less temperature-dependent than the reference bitumen, especially at the midservice temperatures (20–50°C)

(iii) presented three distinct behaviours depending on the temperature range; in fact, CSR showed a similar behaviour with respect to the reference bitumen below 16°C and above 58°C, whereas in the central temperature region, it revealed an opposite tendency (i.e., the increase of the test frequency enhanced the viscous component)

(iv) exhibited an overall lower stiffness with respect to the reference 35/50 pen bitumen

(v) was characterized by a higher fatigue resistance at 20°C than the reference bitumen

(vi) seemed prone to accumulate higher permanent deformations than the reference bitumen at a given high in-service temperatures; however, it should be taken into account that given their particular chromatic characteristic, the clear mixtures will achieve lower temperatures in the field with respect to traditional black surfaces for a given environmental condition; thus, reduced rutting phenomena should be reasonably supposed for CSR-based mixes

Given this summary, it can be concluded that the studied resin demonstrated promising applicability as an innovative binder for road pavement wearing courses, even if a significantly lower structural contribution should be hypothesized, due to its reduced stiffness. Further research could concern the study of the low-temperature behaviour, as well as the analysis of such a product at mixture scale (e.g., a thermal monitoring should be able to quantify the possible temperature mitigation due to the use of clear mixture made with CSR).

Data Availability

Date are available by means of Google Drive system. Files can be downladed at the link https://drive.google.com/file/d/1OBytdtnyrtIcEQGf-60_8FzCA0rK81JV/view?usp=sharing (the password can be obtained from the corresponding author).

Disclosure

Test results and opinions are those of the authors and do not necessarily reflect those of the sponsoring company.

Conflicts of Interest

The authors declare that there are no conflicts of interest regarding the publication of this paper.

Acknowledgments

This study presents a part of the outcomes of a research project funded by the Department of Civil, Environmental and Architectural Engineering (ICEA) of the University of Padua (project no. BIRD168998). This study was also sponsored by Iterchimica Srl (Italy) that gave both financial and technical supports for the research project.

References

[1] H. Higashiyama, M. Sano, F. Nakanishi, O. Takahashi, and S. Tsukuma, "Field measurements of road surface temperature of several asphalt pavements with temperature rise reducing function," *Case Studies in Construction Materials*, vol. 4, pp. 73–80, 2016.

[2] M. Bocci, A. Grilli, F. Cardone, and A. Virgili, "Clear asphalt mixture for wearing course in tunnels: experimental application in the province of bolzano," *Procedia-Social and Behavioral Sciences*, vol. 53, pp. 115–124, 2012.

[3] N. Piérard, J. De Visscher, S. Vansteenkiste, and A. Vanelstraete, "Coloured asphalt pavements: mix design and laboratory performance testing," in *Proceedings of the 8th RILEM International Symposium on Testing and Characterization of Sustainable and Innovative Bituminous Materials*, vol. 11, *RILEM Bookseries*, pp. 283–294, Springer, Ancona, Italy, October 2016.

[4] S. Babić, A. Deluka-Tibljaš, M. Cuculić, and S. Šurdonja, "Analysis of pavement surface heating in urban areas," *Gradevinar*, vol. 64, no. 2, pp. 125–132, 2012.

[5] V. Di Maria, M. Rahman, P. Collins, G. Dondi, and C. Sangiorgi, "Urban heat island effect: thermal response from different types of exposed paved surfaces," *International Journal of Pavement Research and Technology*, vol. 6, no. 4, pp. 414–422, 2013.

[6] Y. Qin, "A review on the development of cool pavements to mitigate urban heat island effect," *Renewable and Sustainable Energy Reviews*, vol. 52, pp. 445–459, 2015.

[7] M. Santamouris, N. Gaitani, A. Spanou, M. Saliari, and K. Vassilakopoulou, "Using cool paving materials to improve microclimate of urban areas—design realization and results of the flisvos project," *Building and Environment*, vol. 53, pp. 128–136, 2012.

[8] P. Weihs, S. Hasel, E. Mursch-Radlgruber et al., "Investigation of the effect of sealed surfaces on local climate in urban areas,"

in *Proceedings of the 9th International Conference on Urban Climate Jointly with 12th Symposium on the Urban Environment*, pp. 1–6, Toulouse, France, July 2015.

[9] K. K. Guan, "Surface and ambient air temperatures associated with different ground material: a case study at the University of California," *Surface and Air Temperatures of Ground Material*, vol. 2011, 2011.

[10] A. Synnefa, T. Karlessi, N. Gaitani et al., "Experimental testing of cool colored thin layer asphalt and estimation of its potential to improve the urban microclimate," *Building and Environment*, vol. 46, no. 6, pp. 38–44, 2011.

[11] F. J. Navarro, P. Partal, F. Martínez-Boza, and C. Gallegos, "Effect of composition and processing on the linear viscoelasticity of synthetic binders," *European Polymer Journal*, vol. 41, no. 6, pp. 1429–1438, 2005.

[12] G. D. Airey, M. H. Mohammed, and C. Fichter, "Rheological characteristics of synthetic road binders," *Fuel*, vol. 87, no. 10-11, pp. 1763–1775, 2008.

[13] F. Merusi and F. Giuliani, "Chromatic and rheological characteristics of clear road binders," *Transportation Research Record: Journal of the Transportation Research Board*, vol. 2293, no. 1, pp. 114–122, 2012.

[14] G. D. Airey and M. H. Mohammed, "Rheological properties of polyacrylates used as synthetic road binders," *Rheologica Acta*, vol. 47, no. 7, pp. 751–763, 2008.

[15] D. Lesueur, "The colloidal structure of bitumen: consequences on the rheology and on the mechanisms of bitumen modification," *Advances in Colloid and Interface Science*, vol. 145, no. 1-2, pp. 42–82, 2009.

[16] C. Efthymiou, M. Santamouris, D. Kolokotsa, and A. Koras, "Development and testing of photovoltaic pavement for heat island mitigation," *Solar Energy*, vol. 130, pp. 148–160, 2016.

[17] J. Yang, Z.-H. Wang, K. E. Kaloush, and H. Dylla, "Effect of pavement thermal properties on mitigating urban heat islands: a multi-scale modeling case study in Phoenix," *Building and Environment*, vol. 108, pp. 110–121, 2016.

[18] J. Chen, H. Wang, and H. Zhu, "Analytical approach for evaluating temperature field of thermal modified asphalt pavement and urban heat island effect," *Applied Thermal Engineering*, vol. 113, pp. 739–748, 2017.

[19] T. Berk, A. Kaufman, and L. Brownston, "A human factors study of color notation systems for computer graphics," *Communications of the ACM*, vol. 25, no. 8, pp. 547–550, 1982.

[20] M. W. Schwarz, W. B. Cowan, and J. C. Beatty, "An experimental comparison of RGB, YIQ, LAB, HSV, and opponent color models," *ACM Transactions on Graphics*, vol. 6, no. 2, pp. 123–158, 1987.

[21] A. R. Smith, "Color gamut transform pairs," *ACM SIGGRAPH Computer Graphics*, vol. 12, no. 3, pp. 12–19, 1978.

[22] D. A. Anderson, D. W. Christensen, B. U. Bahia et al., "Binder characterization, vol. 3: physical properties," SHARP-A-369, p. 475, National Research Council, Washington, DC, USA, 1994.

[23] M. O. Marasteanu and D. A. Anderson, "Establishing linear viscoelastic conditions for asphalt binders," *Transportation Research Record: Journal of the Transportation Research Board*, vol. 1728, no. 1, pp. 1–6, 2000.

[24] M. L. Williams, R. F. Landel, and J. D. Ferry, "The temperature dependence of relaxation mechanisms in amorphous polymers and other glass-forming liquids," *Journal of the American Chemical Society*, vol. 77, no. 14, pp. 3701–3707, 1955.

[25] C. Hintz, R. Velasquez, C. Johnson, and H. Bahia, "Modification and validation of linear amplitude sweep test for binder fatigue specification," *Transportation Research Record: Journal of the Transportation Research Board*, vol. 2207, no. 1, pp. 99–106, 2011.

[26] R. Botella, F. E. Pérez-Jiménez, and R. Miró, "Application of a strain sweep test to assess fatigue behavior of asphalt binders," *Construction and Building Materials*, vol. 36, pp. 906–912, 2012.

[27] M. C. Liao, J. S. Chen, and K. W. Tsou, "Fatigue characteristics of bitumen-filler mastics and asphalt mixtures," *Journal of Materials in Civil Engineering*, vol. 24, no. 7, pp. 916–923, 2011.

[28] A. Al-Haddad, "Fatigue evaluation of Iraqui asphalt binders based on the dissipated energy and viscoelastic continuum damage (VECD) approaches," *Journal of Civil Engineering and Construction Technology*, vol. 6, no. 3, pp. 27–50, 2015.

[29] Y. Kim, H. J. Lee, D. N. Little, and Y. R. Kim, "A simple testing method to evaluate fatigue fracture and damage performance of asphalt mixtures," *Journal of Association of Asphalt Paving Technologists*, vol. 75, pp. 755–788, 2006.

[30] A. Pereira, R. Micaelo, L. Quaresma, and M. T. Cidade, "Evaluation of different methods for the estimation of the bitumen fatigue life with DSR testing," in *RILEM Bookseries*, vol. 11, pp. 1017–1028, Springer, Berlin, Germany, 2016.

[31] C. M. Johnson, *Estimating asphalt binder fatigue resistance using an accelerated test method*, Ph.D. thesis, University of Wisconsin, Madison, WI, USA, 2010.

[32] G. D. Airey, B. Rahimzadh, and A. C. Collop, "Linear viscoelastic limits of bituminous binders," *Association of Asphalt Paving Technologists*, vol. 71, pp. 89–115, 2003.

[33] J. P. Planche, D. Lesueur, and M. Hines, "Evaluation of elastomer modified bitumens using SHRP binder specifications," in *Proceedings of the 1st Eurasphalt and Eurobitume Conference*, pp. 1–17, Strasbourg, France, May 1996.

[34] M. Pasetto, E. Pasquini, G. Giacomello, and A. Baliello, "Innovative pavement surfaces as urban heat islands mitigation strategy: chromatic, thermal and mechanical characterisation of clear/coloured mixtures," *Road Materials and Pavement Design*, vol. 20, no. 1, pp. S533–S555, 2019.